Stronger phonon scattering by larger differences in atomic mass and size in p-type half-Heuslers Hf[subscript 1−x]Ti[subscript x]CoSb[subscript 0.8]Sn[subscript 0.2]

Citation	Yan, Xiao, Weishu Liu, Hui Wang, Shuo Chen, Junichiro Shiomi, Keivan Esfarjani, Hengzhi Wang, Dezhi Wang, Gang Chen, and Zhifeng Ren. "Stronger Phonon Scattering by Larger Differences in Atomic Mass and Size in p-Type Half-Heuslers Hf1−xTixCoSb0.8Sn0.2." Energy & Environmental Science 5, no. 6 (2012): 7543.
As Published	http://dx.doi.org/10.1039/c2ee21554c
Publisher	Royal Society of Chemistry
Version	Author's final manuscript
Citable link	http://hdl.handle.net/1721.1/86909
Terms of Use	Creative Commons Attribution-Noncommercial-Share Alike
Detailed Terms	http://creativecommons.org/licenses/by-nc-sa/4.0/

Stronger phonon scattering by larger differences in atomic mass and size in p-type half-Heuslers $Hf_{1-x}Ti_xCoSb_{0.8}Sn_{0.2}$

Xiao Yan,[a] Weishu Liu,[a] Hui Wang,[a] Shuo Chen,[a] Junichiro Shiomi,[bc] Keivan Esfarjani,[b] Hengzhi Wang,[a] Dezhi Wang,[a] Gang Chen,[*b] and Zhifeng Ren[*a]

[a]Department of Physics, Boston College, Chestnut Hill, Massachusetts 02467, USA

[b]Department of Mechanical Engineering, Massachusetts Institute of Technology, Cambridge, Massachusetts 02139, USA

[c]Department of Mechanical Engineering, University of Tokyo, Tokyo, Japan

Abstract

High lattice thermal conductivity has been the bottleneck for further improvement of thermoelectric figure-of-merit (ZT) of half-Heuslers (HHs) $Hf_{1-x}Zr_xCoSb_{0.8}Sn_{0.2}$. Theoretically the lattice thermal conductivity can be reduced by exploring larger differences in atomic mass and size in the crystal structure, leading to higher ZT. In this paper, we experimentally demonstrated that a lower thermal conductivity in p-type half-Heuslers can indeed be achieved when Ti is used to replace Zr, i.e., $Hf_{1-x}Ti_xCoSb_{0.8}Sn_{0.2}$, due to larger differences in atomic mass and size between Hf and Ti than Hf and Zr. The highest peak ZT, ~1.0 at 800 °C, in the system $Hf_{1-x}Ti_xCoSb_{0.8}Sn_{0.2}$ (x=0.1, 0.2, 0.3, and 0.5) was achieved in $Hf_{0.8}Ti_{0.2}CoSb_{0.8}Sn_{0.2}$, which makes this material practically useful in applications for power generation.

Key words: thermoelectrics, half-Heusler, mass difference, $Hf_{1-x}Ti_xCoSb_{0.8}Sn_{0.2}$

[*]E-mail: gchen2@mit.edu and renzh@bc.edu.

Broader Context

How to scavenge the vast amount of waste heat has increasingly become a major concern. Possibly, thermoelectrics can provide an economical and environmentally friendly way to achieve this. High thermoelectric figure-of-merit (ZT) materials are preferred for efficient performance. Historically, PbTe and skutterudites have been considered the candidates for medium temperature applications owing to their good ZT values. However, their uses are limited owing to either toxicity or low thermal stability. In the same temperature range, half-Heuslers are chemically non-toxic and thermally stable compared with the PbTe and skutterudites but the peak ZT of p-type half-Heuslers has remained around 0.5 for quite a long time till our recent work that improved the ZT to 0.8. In this work, we achieved ZT about 1 for p-type half-Heusler, which makes it practically useful for medium to high temperature power generation applications, such as waste heat recovery in car exhaust system. Specifically, the ZT enhancement mainly comes from the reduction of thermal conductivity, which arises partly from the enhanced alloy scattering due to larger differences in atomic mass and size of Hf and Ti than Hf and Zr and partly from enhanced boundary scattering due to various nanostructures.

Introduction

Thermoelectric (TE) materials can convert heat, such as that in the vehicle exhaust systems[1,2] and that generated from solar radiations[3-5], into electric power in an environmentally friendly and less costly way. PbTe[6,7] and skutterudites[8] are the suitable materials for medium temperature (300-500 °C) whereas SiGe[9,10] alloys are for high temperature power generation applications (500-800 °C). Despite the advantages of non-toxicity, high thermal stability, and low cost compared to PbTe, skutterudites, and SiGe alloys, half-Heuslers[11], another class of thermoelectric materials, have been much less explored, owing to the low thermoelectric figure-of-merit (ZT). By definition, $ZT = \left(\dfrac{S^2\sigma}{\kappa} \right) T$, where S is the Seebeck coefficient, $\boldsymbol{\sigma}$ the electrical conductivity, $\boldsymbol{\kappa}$ the thermal conductivity, and T the absolute temperature. Historically, peak ZT of p-type half-Heuslers remains low ~0.5, mostly attributed to the high thermal conductivity[12]. Only recently, peak ZT of 0.8 at 700 °C has been achieved in p-type half-Heusler system by nanostructure approach[13], revealing the potential of half-Heuslers as promising candidate for high-temperature power generation applications. In this report, we found that larger differences in atomic mass and size between Hf and Ti than Hf and Zr can further reduce the lattice thermal conductivity, leading to ZT of ~1.0 in any p-type HH materials, which makes HHs really interesting for being considered of power generation applications in the temperature range up to 800 °C, possibly replacing the much more expensive SiGe alloys[9,10].

Alloy scattering resulting from differences in atomic mass and size may effectively lower the lattice thermal conductivity[14]. In the case of p-type half-Heuslers with the formula MCoSb, where M is Ti or Zr or Hf or the combination of two or three, the high substitutability of the three lattice sites (M, Co, and Sb) provides ample opportunities to further depress the thermal conductivity. There have been some initial reports on reducing thermal conductivity via elemental substitution at the three respective lattice sites of p-type half-Heuslers, such as combination of Ti and Zr (M site)[15,16], substitution of Co by Fe[17], Ir[18], or Rh[19], and Sb by Sn[20,21,22] or Ge[23]. Some theoretical calculations have been conducted to investigate the effect of mass difference and strain field fluctuation on lattice thermal conductivity of half-Heuslers as well[24,25]. A combination of Hf and Ti is supposed to be more effective in reducing the lattice thermal conductivity than that of Hf and Zr, considering the larger differences in atomic mass

3

and size of Hf and Ti. This concept has been validated experimentally in n-type (Ti, Zr, Hf)NiSn half-Heusler systems[26]. However, there is lack of knowledge about the effect of (Hf, Ti) combination on the thermal conductivity and ZT of p-type half-Heuslers. Our initial motivation is that enhanced alloy scattering of phonons by larger atomic mass and size differences in combination with the enhanced boundary scattering by nanocomposite approach could further reduce the still large lattice part of thermal conductivity without too much penalty on the electronic properties, thereby enhancing ZT. Our investigation on the thermoelectric properties of $Hf_{1-x}Ti_xCoSb_{0.8}Sn_{0.2}$ (x=0.1, 0.2, 0.3, and 0.5) proves that $Hf_{0.8}Ti_{0.2}CoSb_{0.8}Sn_{0.2}$ has indeed a lower thermal conductivity ~2.7 $Wm^{-1}K^{-1}$ leading to a higher ZT ~1.0 at 800 ^{o}C.

Experimental Procedure

Alloyed ingots with compositions $Hf_{1-x}Ti_xCoSb_{0.8}Sn_{0.2}$ (x=0.1, 0.2, 0.3, and 0.5, all compositions are nominal) were first formed by arc melting a mixture of appropriate amount of individual elements according to the stoichiometry. To prevent oxidation during arc melting, the chamber was continuously flown with Ar gas throughout the operation. Normally we re-melt the ingot twice with each time flipping over the ingot to ensure the homogeneity of as-arc-melted ingot (we notice that there is minor Sb loss, however additional effort compensating the loss did not result in better thermoelectric properties). Then the ingot was loaded into a ball milling jar with grinding balls inside an argon-filled glove box and then subjected to a mechanical ball-milling process to make nanopowders. Finally bulk samples were obtained by consolidating the nanopowders into cylinders with a diameter of 12.7 mm and a height of 13 mm, using the direct current induced hot-press method, for us to measure all properties in the same direction.

X-ray diffraction (XRD) (PANalytical X'Pert Pro) analysis with a wavelength of 0.154 nm (Cu Kα) was performed on as-pressed samples with different Hf/Ti ratios. The freshly fractured surface of as-pressed $Hf_{0.8}Ti_{0.2}CoSb_{0.8}Sn_{0.2}$ samples was observed by a scanning electron microscope (SEM, JEOL 6340F) and a high resolution transmission electron microscope (HRTEM, JEOL 2010F).

To measure the thermoelectric properties of bulk samples, bars of about $2 \times 2 \times 12$ mm and disks of 12.7 mm in diameter and 2 mm in thickness were made. The bar samples were used to measure the electrical conductivity and Seebeck coefficient on a commercial equipment (ULVAC, ZEM3). The disk samples were used to obtain the thermal conductivity, which is calculated as the product of thermal diffusivity, specific heat, and volumetric density. The volumetric density was measured using an Archimedes' kit. The specific heat was determined by a High-Temperature DSC instrument (404C, Netzsch Instruments, Inc.). The thermal diffusivity was measured using a laser flash system (LFA 457 Nanoflash, Netzsch Instruments, Inc.). The uncertainties are 3% for electrical conductivity, thermal diffusivity, and specific heat, and 5% for the Seebeck coefficient, leading to an 11% uncertainty in ZT.

We have repeated the experiments many times and have confirmed that the peak ZT values were reproducible within experimental errors. Besides, we measured the same sample up to 800 ^{o}C again after the first measurement and found that there was no degradation in both individual properties and the ZT.

Results and Discussions

Figure 1a shows the XRD patterns of the as-pressed $Hf_{1-x}Ti_xCoSb_{0.8}Sn_{0.2}$ (x=0.1, 0.2, 0.3, and 0.5) samples. The diffraction peaks of all samples are well-matched with those of cubic half-Heusler phases[12]. No noticeable impurity phases are observed. A close scrutiny reveals that XRD peaks shift towards higher angles with increasing Ti, suggesting that Ti replace the Hf to form alloys. We have also estimated the lattice parameter a of all samples with different Hf/Ti ratios and plotted the results with respect to Ti fraction x in Fig. 1b. As expected, the lattice parameter decreases linearly with increasing Ti, following the Vegard's law.

The SEM image of the as-pressed $Hf_{0.8}Ti_{0.2}CoSb_{0.8}Sn_{0.2}$ sample is displayed in Fig. 2a, from which we can see that the grain sizes are in the range of 50-300 nm with an estimated average size about 100-200 nm. The TEM image (Fig. 2b) confirms the average grain size observed from the SEM image, which is ~200 nm and below. Figure 2c shows two nanodots

sitting on the grain boundaries. These nanodots are commonly observed inside our samples. One unique feature pertaining to our samples is that dislocations are also common, as shown in Fig. 2d. The origin of the dislocations is probably due to the extensive mechanical deformation during ball milling. The small grains, nanodots, and dislocations are all favorable for a low lattice thermal conductivity due to enhanced phonon scattering.

Figure 3 shows the temperature-dependent thermoelectric (TE) properties of $Hf_{1-x}Ti_xCoSb_{0.8}Sn_{0.2}$ (x=0.1, 0.2, 0.3, and 0.5) samples. All these samples have been made by ball milling the as-arc-melted ingot using the same ball milling time and hot pressing conditions. The electrical conductivities are plotted in Fig. 3a, from which we can see that electrical conductivity decreases with increasing Ti for the whole temperature range. The positive signs of Seebeck coefficients of all samples indicate p-type transport behavior (Fig. 3b). The Seebeck coefficient follows roughly the trend of increasing with increasing of Ti, opposite to the trend of electrical conductivity (Fig. 3b). Meanwhile, the differences in Seebeck coefficients among various compositions are diminished at elevated temperatures. Figure 3c demonstrates the temperature-dependent power factor. $Hf_{0.9}Ti_{0.1}CoSb_{0.8}Sn_{0.2}$ has the highest power factor whereas $Hf_{0.5}Ti_{0.5}CoSb_{0.8}Sn_{0.2}$ has the lowest power factor for the whole temperature range. The power factor of $Hf_{0.8}Ti_{0.2}CoSb_{0.8}Sn_{0.2}$ increases steadily with temperature and reaches as high as 25.7×10^{-4} $Wm^{-1}K^{-2}$ at 800 °C.

Figure 3d shows the temperature-dependent total thermal conductivity of $Hf_{1-x}Ti_xCoSb_{0.8}Sn_{0.2}$ (x=0.1, 0.2, 0.3, and 0.5) samples. The volumetric densities of $Hf_{1-x}Ti_xCoSb_{0.8}Sn_{0.2}$ samples are 10.1, 9.8, 9.7, and 9.0 gcm^{-3} for x=0.1, 0.2, 0.3, and 0.5, respectively, which are 98%, 98%, 99.9%, and 99.6% of the theoretical density according to each composition. For the whole temperature range, thermal conductivities of $Hf_{0.8}Ti_{0.2}CoSb_{0.8}Sn_{0.2}$, $Hf_{0.7}Ti_{0.3}CoSb_{0.8}Sn_{0.2}$, and $Hf_{0.5}Ti_{0.5}CoSb_{0.8}Sn_{0.2}$ samples are similar with each other and much lower than that of $Hf_{0.9}Ti_{0.1}CoSb_{0.8}Sn_{0.2}$. The thermal conductivity of $Hf_{0.8}Ti_{0.2}CoSb_{0.8}Sn_{0.2}$ changes very little with increasing temperature and the minimum value is 2.7 $Wm^{-1}K^{-1}$. To get a clear view of how Hf/Ti ratio affects the lattice heat transport, we estimated the lattice thermal conductivity (κ_l) by subtracting both the electronic contribution (κ_e) and the bipolar contribution ($\kappa_{bipolar}$) from the total thermal conductivity (κ) while κ_e was obtained using the Wiedemann-

Franz law. The temperature dependent Lorenz number was calculated from the reduced Fermi energies[27], which were estimated from the Seebeck coefficient with a consideration of the two-band model. Similar with the total thermal conductivity, lattice thermal conductivities of $Hf_{0.8}Ti_{0.2}CoSb_{0.8}Sn_{0.2}$, $Hf_{0.7}Ti_{0.3}CoSb_{0.8}Sn_{0.2}$, and $Hf_{0.5}Ti_{0.5}CoSb_{0.8}Sn_{0.2}$ samples are similar with each other and much lower than that of $Hf_{0.9}Ti_{0.1}CoSb_{0.8}Sn_{0.2}$ (Fig. 3e). As Ti is gradually introduced into $HfCoSb_{0.8}Sn_{0.2}$ system, lattice thermal conductivity experiences a sharp suppression from x=0.1 to x=0.2 and then becomes almost saturated above x=0.2. The theoretical calculations on $Hf_{1-x}Ti_xCoSb$ using molecular dynamics (MD) simulations via the harmonic and cubic force interatomic constants obtained from first principles calculations predicted such thermal conductivity decrease[28]. The lattice thermal conductivities of $Hf_{1-x}Ti_xCoSb_{0.8}Sn_{0.2}$ (x=0.1, 0.2, 0.3, and 0.5) samples at room temperature are plotted in the inset of Fig. 3e in comparison with the calculations. It is very encouraging to see that our experimental data and the theoretical calculations are in very good agreement.

Because of the low thermal conductivity and high power factor achieved by partially substituting Hf with Ti, ZT of $Hf_{0.8}Ti_{0.2}CoSb_{0.8}Sn_{0.2}$ reached 1.0 at 800 ^{o}C and 0.9 at 700 ^{o}C (Fig. 3f), showing promise for p-type material as an option in high temperature applications.

We also show the specific heat (Fig. 4a) and thermal diffusivity (Fig. 4b) of $Hf_{1-x}Ti_xCoSb_{0.8}Sn_{0.2}$ (x=0.1, 0.2, 0.3, and 0.5) samples. The specific heat of all samples increases steadily with temperature. For the same temperature, the specific heat increases with increasing Ti. To be cautious, we measured the specific heat of $Hf_{0.8}Ti_{0.2}CoSb_{0.8}Sn_{0.2}$, which has the highest ZT at high temperatures, both by a High-Temperature DSC instrument (404C, Netzsch Instruments, Inc.), which can measure the sample beyond 800 ^{o}C, and by a Low-Temperature DSC instrument (200-F3, Netzsch Instruments, Inc.), which can only reach up to 600 ^{o}C. It turns out that measurement results from two different DSC instruments agree with each other within 3%. On the other hand, thermal diffusivity of all samples exactly follows the trend of decreasing with increasing Ti.

We also plotted the temperature-dependent TE properties of nanostructured bulk sample $Hf_{0.8}Ti_{0.2}CoSb_{0.8}Sn_{0.2}$ in comparison with that of $Hf_{0.5}Zr_{0.5}CoSb_{0.8}Sn_{0.2}$[13] in Fig. 5. Both samples

have been subjected to the same ball milling and hot pressing conditions to minimize the size effect on the transport properties. The electrical conductivity of $Hf_{0.5}Zr_{0.5}CoSb_{0.8}Sn_{0.2}$ is higher than that of $Hf_{0.8}Ti_{0.2}CoSb_{0.8}Sn_{0.2}$ for the whole temperature range and the difference becomes smaller with increasing temperature (Fig. 5a). In contrast, the Seebeck coefficient of $Hf_{0.8}Ti_{0.2}CoSb_{0.8}Sn_{0.2}$ is almost the same with that of $Hf_{0.5}Zr_{0.5}CoSb_{0.8}Sn_{0.2}$ for all the temperatures (Fig. 5b). As a result of the reduced electrical conductivity, the power factor of $Hf_{0.8}Ti_{0.2}CoSb_{0.8}Sn_{0.2}$ is lower than that of $Hf_{0.5}Zr_{0.5}CoSb_{0.8}Sn_{0.2}$ from 100 ^{o}C to 700 ^{o}C (Fig. 5c). However, this reduced power factor is compensated by the much reduced thermal conductivity (Fig. 5d), which yields an enhanced ZT especially at higher temperatures (Fig. 5f). The total thermal conductivity of $Hf_{0.8}Ti_{0.2}CoSb_{0.8}Sn_{0.2}$ is ~17% lower than that of $Hf_{0.5}Zr_{0.5}CoSb_{0.8}Sn_{0.2}$ (Fig. 5d), indicating that the combination of Hf and Ti is more effective in reducing thermal conductivity than the combination of Hf and Zr. The origin of the thermal conductivity reduction achieved in $Hf_{0.8}Ti_{0.2}CoSb_{0.8}Sn_{0.2}$ in comparison with $Hf_{0.5}Zr_{0.5}CoSb_{0.8}Sn_{0.2}$ comes from two parts: electronic part and lattice part. Specifically, κ_e of $Hf_{0.8}Ti_{0.2}CoSb_{0.8}Sn_{0.2}$ is about 13%-31% lower than that of $Hf_{0.5}Zr_{0.5}CoSb_{0.8}Sn_{0.2}$. The lattice thermal conductivity of $Hf_{0.8}Ti_{0.2}CoSb_{0.8}Sn_{0.2}$ is about 11-19% lower than that of $Hf_{0.5}Zr_{0.5}CoSb_{0.8}Sn_{0.2}$ (Fig. 5e), consistent with the effect of more thermal conductivity reduction by Hf and Ti combination in n-type half-Heusler system[26]. Our experimental results clearly show that thermal conductivity can be most effectively reduced in the combination of Hf and Ti, owing to the larger difference in atomic mass and size in the case of Hf and Ti combination. However, the lattice part still dominates the total thermal conductivity. If more alloy scattering and/or more boundary scattering by even smaller grains can be achieved, thermal conductivity is expected to be even more reduced. It is clearly shown in Fig. 5f that the ZT of $Hf_{0.8}Ti_{0.2}CoSb_{0.8}Sn_{0.2}$ is comparable to that of $Hf_{0.5}Zr_{0.5}CoSb_{0.8}Sn_{0.2}$ at low temperatures and exceeds that of $Hf_{0.5}Zr_{0.5}CoSb_{0.8}Sn_{0.2}$ at temperatures above 500 ^{o}C (Fig. 5f), demonstrating promise for high temperature applications. Data of p-type silicon germanium (SiGe)[10], another promising p-type material for high temperature applications, are also included for comparison (Fig. 5f). $Hf_{0.8}Ti_{0.2}CoSb_{0.8}Sn_{0.2}$ may also have cost advantages over SiGe due to the extremely high cost of Ge.

The data we report here are the representative results from many runs. A few typical ZT vs. T curves of $Hf_{0.8}Ti_{0.2}CoSb_{0.8}Sn_{0.2}$ are shown in Fig. 6 to demonstrate the repeatability. We

have not only made many parallel batches under the similar conditions (samples 1 and 2) but also did the thermal stability test by measuring the same sample up to 800 $^{\circ}$C again after the first measurement (sample 1 and 1re). In fact, the results are repeatable within 10% from batch to batch and there is no observable degradation in either individual properties or ZT after re-measurement to 800 $^{\circ}$C. The good repeatability and thermal stability of $Hf_{0.8}Ti_{0.2}CoSb_{0.8}Sn_{0.2}$ sample further strengthen its promising candidacy for high temperature applications.

Although we have optimized the binary $Hf_{1-x}Ti_xCoSb_{0.8}Sn_{0.2}$ composition by tuning Hf/Ti ratio and demonstrated the feasibility of thermal conductivity reduction and ZT enhancement, there still remains much room for further improvement. First, a ternary combination of Ti, Zr, and Hf at M site has given rise to a ZT value of 0.92 in n-type MNiPdSnSb system[29]. However, there is little understanding about the influence of ternary combination of Ti, Zr, and Hf on the transport properties of p-type half-Heuslers, which deserves further investigation. Second, boundary scattering can be enhanced more by preserving nanosize of the precursor nanopowders during hot pressing. Combining enhanced alloying scattering along with enhanced boundary scattering, thermal conductivity is expected to be lowered even more and ZT is most likely to reach even higher.

Conclusions

Larger differences in atomic mass and size between Hf and Ti than Hf and Zr at M site of p-type half-Heuslers MCoSb are proved effective on reducing the lattice thermal conductivity by stronger phonon scattering, which leads to a lower thermal conductivity of 2.7 $Wm^{-1}K^{-1}$ in $Hf_{0.8}Ti_{0.2}CoSb_{0.8}Sn_{0.2}$. As a result, a peak ZT of $Hf_{0.8}Ti_{0.2}CoSb_{0.8}Sn_{0.2}$ reached 1.0 at 800 $^{\circ}$C, which paves the way for consideration of real practical applications of HHs for power generation applications.

Acknowledgment

References

1. L. E. Bell, *Science*, 2008, **321**, 1457.

2. J. H. Yang and F. R. Stabler, *J. Electron. Mater.*, 2009, **38**, 1245-1251.

3. M. Telkes, *J. Appl. Phys.*, 1954, **25**, 765-777.

4. D. Mills, *Sol. Energy*, 2004, **76**, 19-31.

5. D. Kraemer, B. Poudel, H. –P. Feng, J. C. Caylor, B. Yu, X. Yan, Y. Ma, X. W. Wang, D. Z. Wang, A. Muto, K. McEnaney, M. Chiesa, Z. F. Ren and G. Chen, *Nature Mater.*, 2011, **10**, 532-538.

6. J. P. Heremans, V. Jovovic, E. S. Toberer, A. Saramat, K. Kurosaki, A. Charoenphakdee, S. Yamanaka and G. J. Snyder, *Science*, 2008, **321**, 554-557.

7. Y. Z. Pei, X. Y. Shi, A. LaLonde, H. Wang, L. D. Chen and G. J. Snyder, *Nature*, 2011, **473**, 66-69.

8. B. C. Sales, D. Mandrus and R. K. Williams, *Science*, 1996, **272**, 1325-1328.

9. X. W. Wang, H. Lee, Y. C. Lan, G. H. Zhu, G. Joshi, D. Z. Wang, J. Yang, A. J. Muto, M. Y. Tang, J. Klatsky, S. Song, M. S. Dresselhaus, G. Chen and Z. F. Ren, *Appl. Phys. Lett.*, 2008, **93**, 193121-1.

10. G. Joshi, H. Lee, Y. C. Lan, X. W. Wang, G. H. Zhu, D. Z. Wang, R. W. Gould, D. C. Cuff, M. Y. Tang, M. S. Dresselhaus, G. Chen and Z. F. Ren, *Nano Lett.*, 2008, **8**, 4670.

11. S. J. Poon, in *Recent Trends in Thermoelectric Materials Research II, Semiconductors and Semimetals*, Ed. T. M. Tritt, Academic, New York, 2001, vol. 70, pp. 37.

12. S. R. Culp, J. W. Simonson, S. J. Poon, V. Ponnambalam, J. Edwards and T. M. Tritt, *Appl. Phys. Lett.*, 2008, **93**, 022105.

13. X. Yan, G. Joshi, W. S. Liu, Y. C. Lan, H. Wang, S. Lee, J. W. Simonson, S. J. Poon, T. M. Tritt, G. Chen and Z. F. Ren, *Nano Lett.*, 2011, **11**, 556-560.

14. G. A. Slack, *Phys. Rev.*, 1957, **105**, 829.

15. W. J. Xie, X. F. Tang and Q. J. Zhang, *Chin. Phys.*, 2007, **16**, 3549-04.

16. V. Ponnambalam, P. N. Alboni, J. Edwards, T. M. Tritt, S. R. Culp and S. J. Poon, *J. Appl. Phys.*, 2008, **103**, 063716.

17. T. Wu, W. Jiang, X. Y. Li, Y. F. Zhou and L. D. Chen, *J. Appl. Phys.*, 2007, **102**, 103705.

18. N. J. Takas, P. Sahoo, D. Misra, H. F. Zhao, N. L. Henderson, K. Stokes and P. F. P. Poudeu, *J. Electron. Mater.*, 2011, **40**, 662.

19. P. Maji, N. J. Takas, D. K. Misra, H. Gabrisch, K. Stokes and P. F. P. Poudeu, *J. Solid State Chem.*, 2010, **183**, 1120.

20. T. Sekimoto, K. Kurosaki, H. Muta and S. Yamanaka, *J. Alloys Compd.*, 2006, **407**, 326-329.

21. T. Sekimoto, K. Kurosaki, H. Muta and S. Yamanaka, *Jpn. J. Appl. Phys.*, 2007, **46**, L673-L675.

22. Y. Xia, S. Bhattacharya, V. Ponnambalam, A. L. Pope, S. J. Poon and T. M. Tritt, *J. Appl. Phys.*, 2000, **88**, 1952.

23. T. Wu, W. Jiang, X. Y. Li, S. Q. Bai, S. C. Liufu and L. D. Chen, *J. Alloys Compd.*, 2009, **467**, 590.

24. J. Yang, G. P. Meisner and L. Chen, *Appl. Phys. Lett.*, 2004, **85**, 1140.

25. M. Zhou, L. D. Chen, W. Q. Zhang and C. Feng, *J. Appl. Phys.*, 2005, **98**, 013708.

26. Y. Kimura, Y. Ueno and Y. Mishima, *J. Electron. Mater.*, 2009, **38**, 934.

27. W. S. Liu, Q. Y. Zhang, Y. C. Lan, S. Chen, X. Yan, Q. Zhang, H. Wang, D. Z. Wang, G. Chen and Z. F. Ren, *Adv. Energy Mater.*, 2011, **1**, 577-587.

28. J. Shiomi, K. Esfarjani and G. Chen, *Phys. Rev. B*, 2011, **84**, 104302.

29. P. J. Lee, S. C. Tseng and L. S. Chao, *J. Alloys Compd.*, 2010, **496**, 620-623.

Figure Captions

Fig. 1.   (a) XRD patterns and (b) lattice parameters extracted from XRD patterns of as-pressed $Hf_{1-x}Ti_xCoSb_{0.8}Sn_{0.2}$ (x=0.1, 0.2, 0.3 and 0.5) samples.

Fig. 2.   (a) SEM image and (b-d) TEM images of as-pressed $Hf_{0.8}Ti_{0.2}CoSb_{0.8}Sn_{0.2}$ sample.

Fig. 3.   Temperature-dependent (a) electrical conductivity, (b) Seebeck coefficient, (c) power factor, (d) thermal conductivity, (e) lattice thermal conductivity and (f) ZT of $Hf_{1-x}Ti_xCoSb_{0.8}Sn_{0.2}$ (x=0.1, 0.2, 0.3 and 0.5) samples. The lattice thermal conductivities of $Hf_{1-x}Ti_xCoSb_{0.8}Sn_{0.2}$ (x=0.1, 0.2, 0.3 and 0.5) samples at room temperature are plotted in comparison with Prof. Jun's molecular dynamics (MD) calculations on $Hf_{1-x}Ti_xCoSb$ in the inset of Fig. 3e.

Fig. 4.   Temperature-dependent (a) specific heat and (b) thermal diffusivity of $Hf_{1-x}Ti_xCoSb_{0.8}Sn_{0.2}$ (x=0.1, 0.2, 0.3 and 0.5) samples.

Fig. 5.   Temperature-dependent (a) electrical conductivity, (b) Seebeck coefficient, (c) power factor, (d) thermal conductivity, (e) lattice thermal conductivity and (f) ZT of $Hf_{0.8}Ti_{0.2}CoSb_{0.8}Sn_{0.2}$ and $Hf_{0.5}Zr_{0.5}CoSb_{0.8}Sn_{0.2}$[13]. ZT of p-type SiGe (Ref. 10) is also included in Fig. 5f for comparison.

Fig. 6.   Repeatability demonstration of $Hf_{0.8}Ti_{0.2}CoSb_{0.8}Sn_{0.2}$ reflected on ZT dependence of temperature from different batches and from thermal stability test.
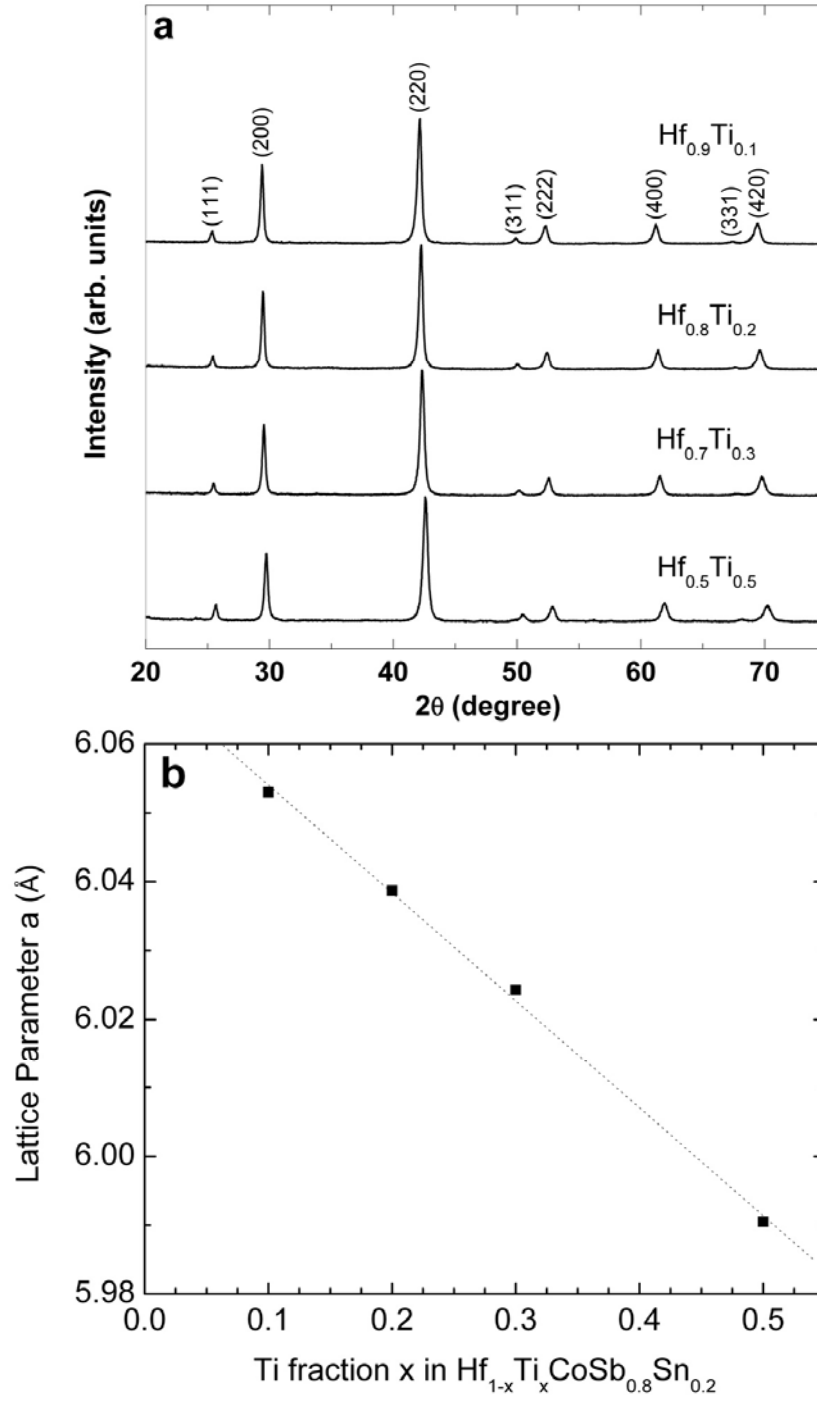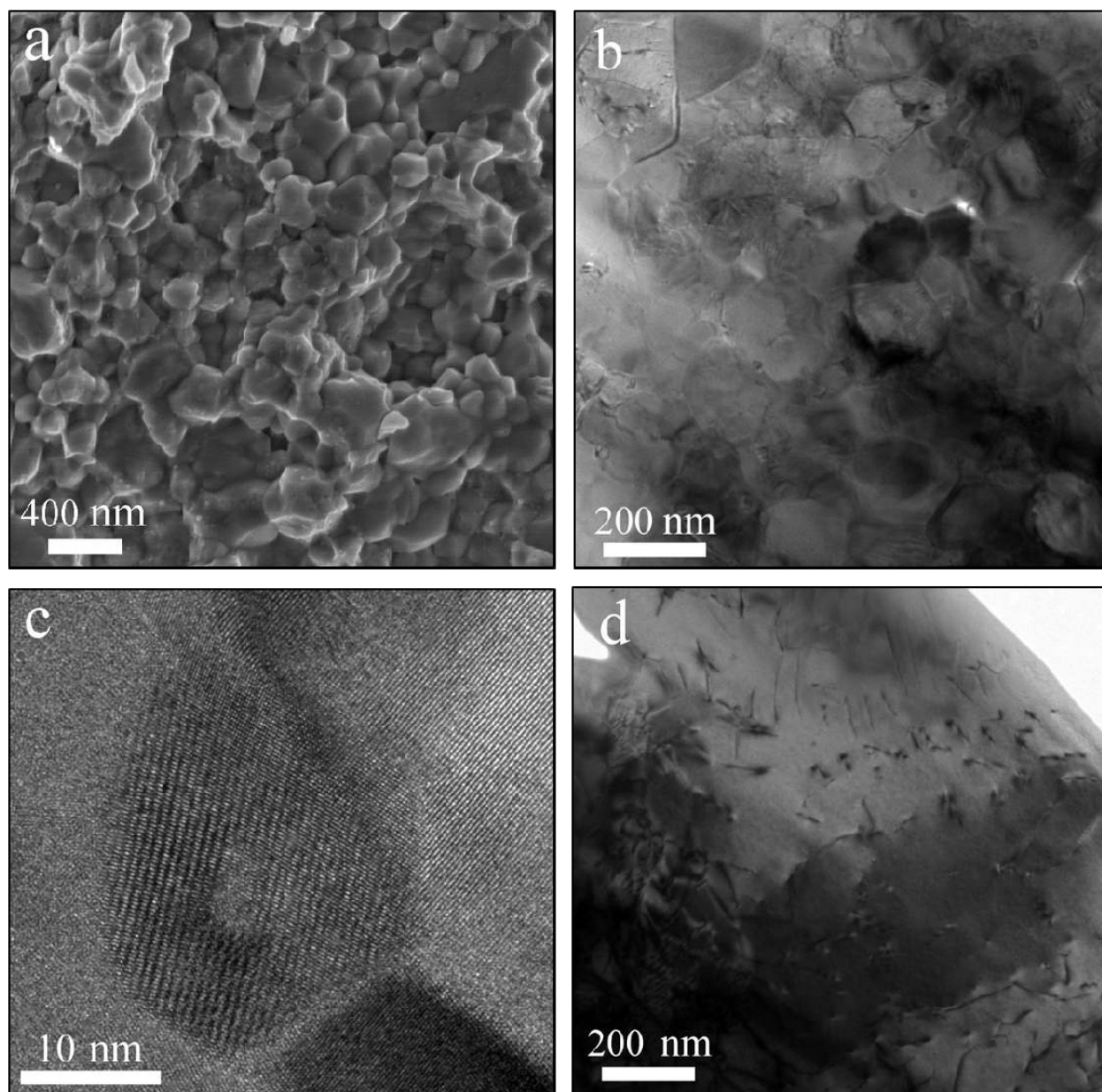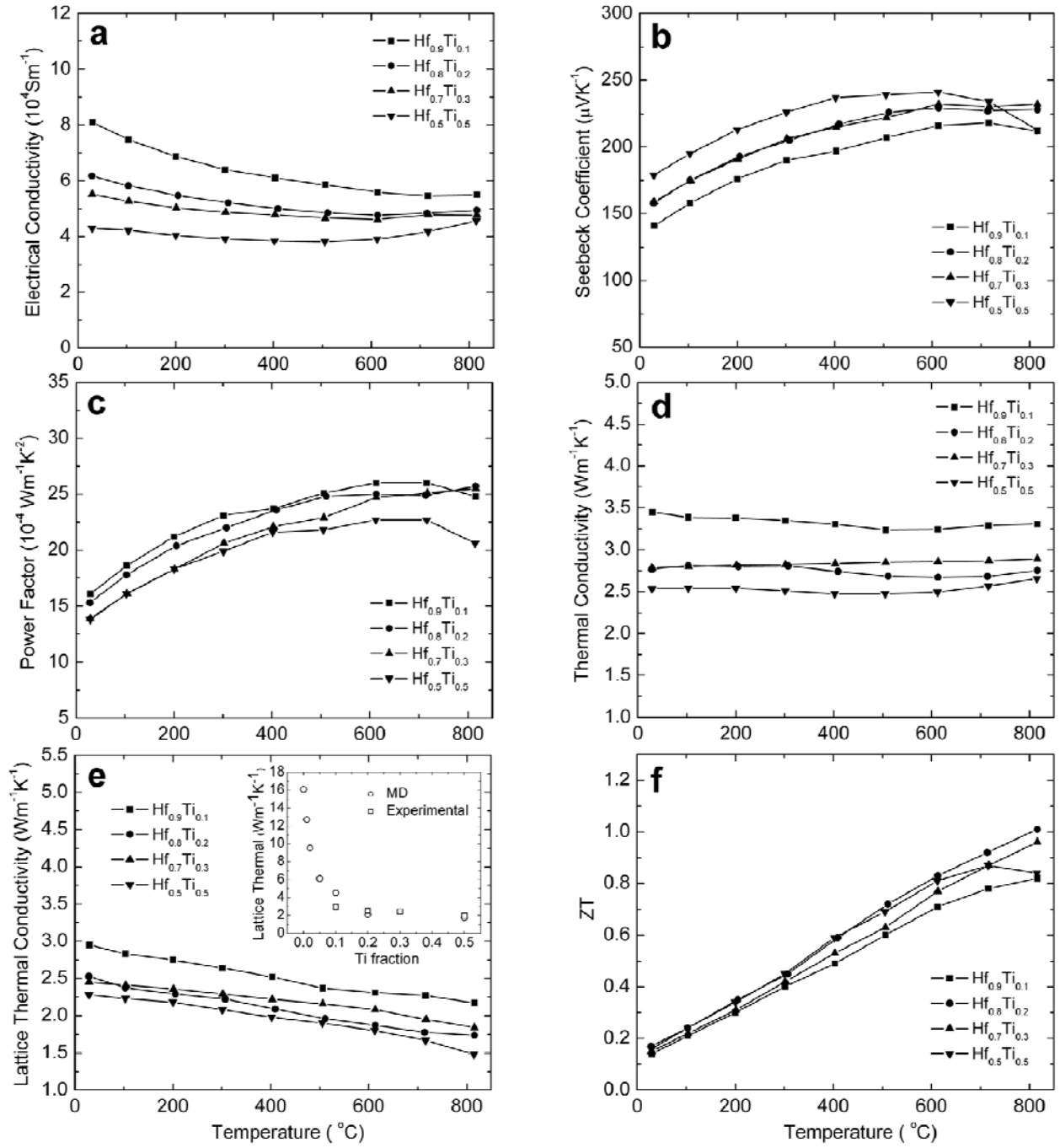
Fig. 1 Xiao Yan *et al.*

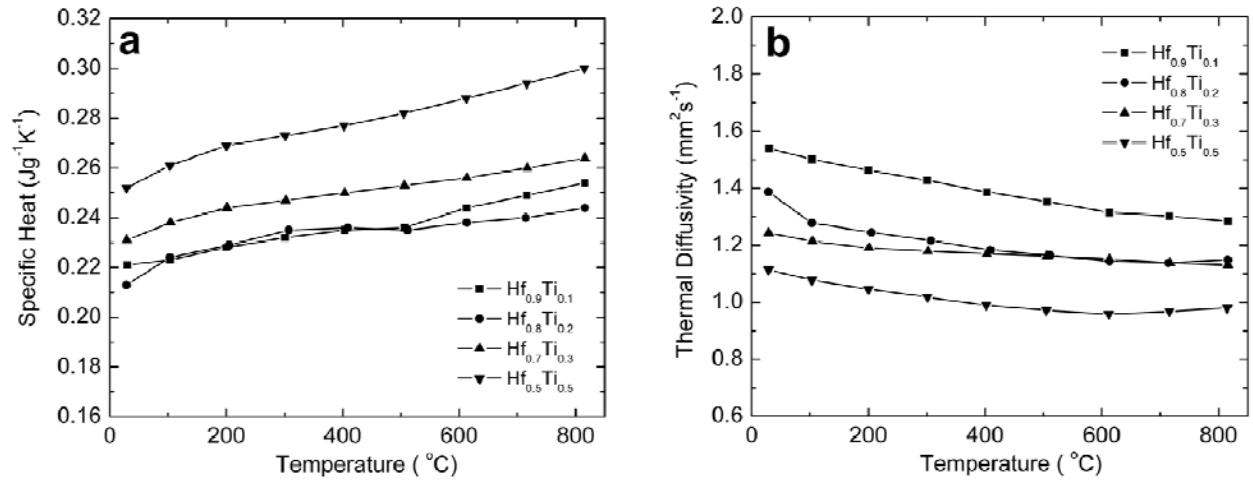**Fig. 2 Xiao Yan** *et al.*
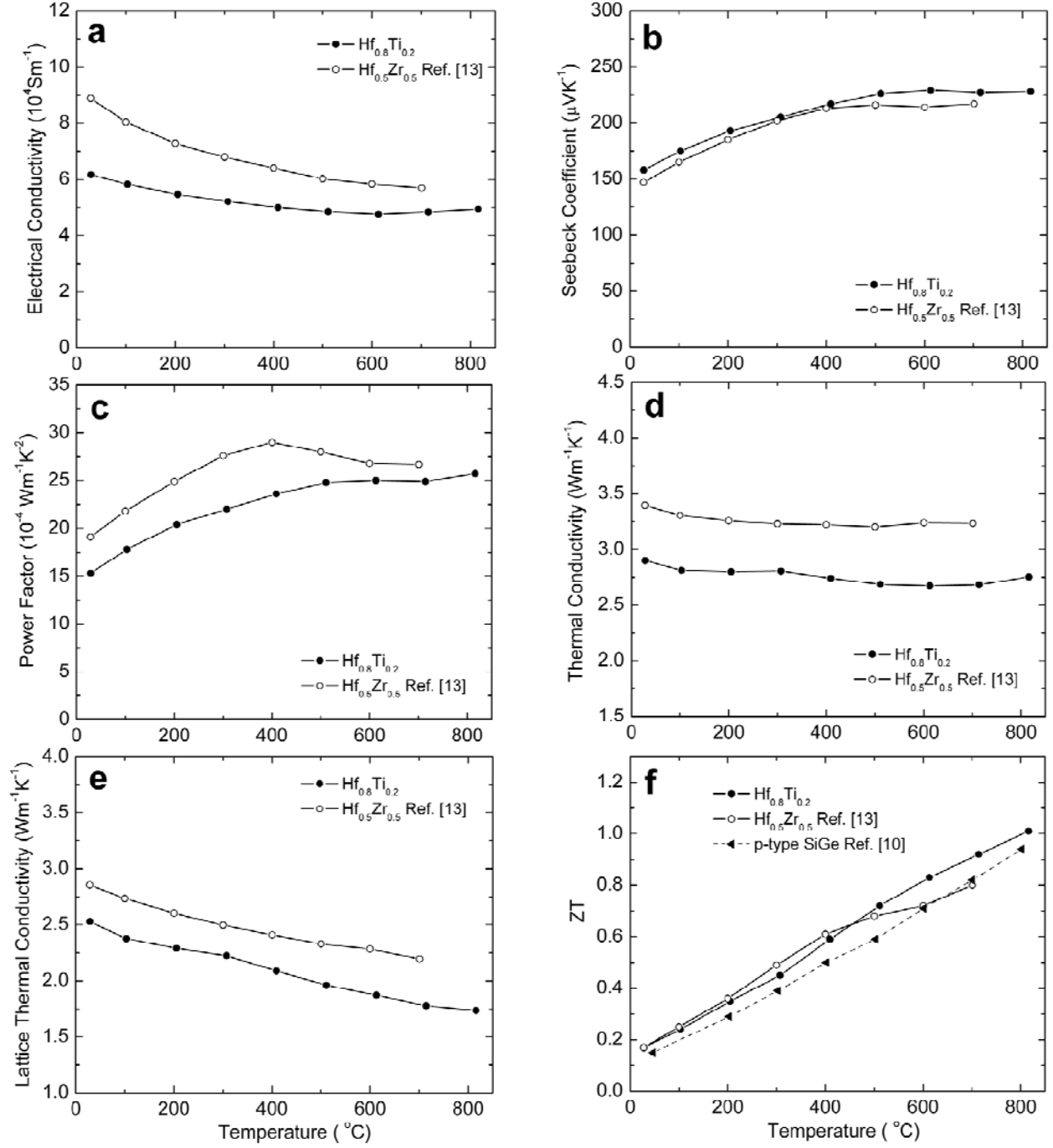
Fig. 3 Xiao Yan *et al.*

Fig. 4 Xiao Yan *et al*.
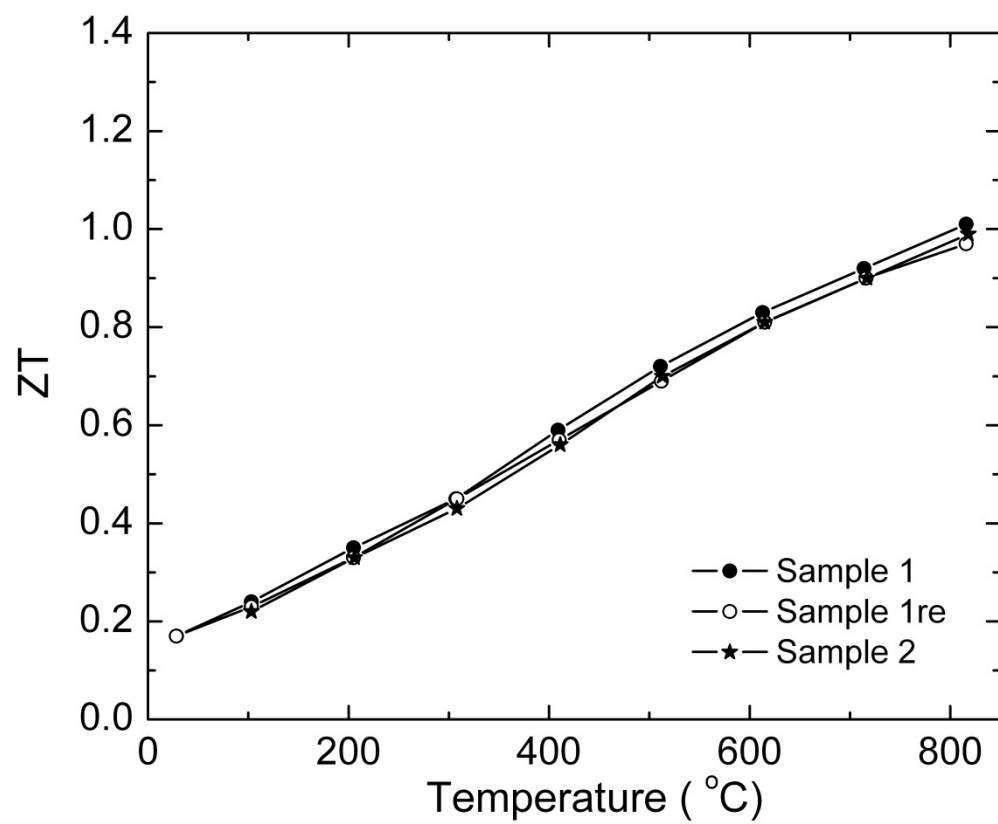
Fig. 5 Xiao Yan *et al.*

Fig. 6 Xiao Yan *et al.*